

An Automated Finite Element Mesh Generation and Element Coding in 2-D Electromagnetic Inversion

S.P. Sharma and P. Kaikkonen

Department of Geophysics, University of Oulu,
FIN-90570 Oulu, Finland

(Received: December 1997; Accepted: August 1998)

Abstract

An automated mesh generation and element coding in finite element modelling is developed for the optimisation of geometrical and physical model parameters of the 2-D structures. The approach is based on an automatic reconstruction of the mesh and the element codes for varying geometrical and physical parameters of the subsurface during the optimisation process. The efficacy of the approach is demonstrated through its application in forward modelling and inversion of the VLF electromagnetic data from the simple and complex subsurface structures.

Key words: finite element method, automated mesh generation, 2-D electromagnetic inversion

1. Introduction

Mesh generation is an essential part of any numerical approach in which a true structure of the domain under research is replaced by the one for which a numerical approximation to a partial differential equation can be made and evaluated. For the electromagnetic (EM) methods in studying the solid Earth the subsurface structure must be discretized into the mesh and the Maxwell's equations must be solved numerically in that mesh. Mesh design for a given model is generally done manually on the basis of the *a priori* knowledge of skin depths in different conductivities of the model. This restricts the interpreter to do only forward modelling or at least not more than the trial and error inversion, because an advanced inversion is too limited without a possibility to do an automatic mesh reconstruction during the inversion process. Several studies reported in literature regarding the electromagnetic inversion utilising some of the numerical techniques, e.g., the integral equation method (IEM), the finite-difference method (FDM) or the finite element method (FEM) for a forward solution have used a fixed mesh (e.g., *Weidelt, 1975; Jupp and Vozoff, 1977; Oristaglio and Worthington, 1980; Zhdanov and Varentsov, 1983*). Therefore, there has been some sort of limitation in the inversion fixing either the geometry or physical parameters of the inhomogeneities. In such situations it is difficult to get true and reliable estimates of

either parameters. However, the reliable and well working iterative inversions based on the FEM, FDM or IEM methods in forward modelling, need the mesh to be reconstructed automatically depending on the geometrical and physical parameters of the subsurface during the course of the inversion process.

A finite element model can represent almost an arbitrary complex subsurface. Several FEM studies with EM data have been reported since the beginning of the 1970's (e.g., *Coggon*, 1971; *Reddy and Rankin*, 1973; *Rodi*, 1976; *Kaikkonen*, 1977; *Pridmore et al.*, 1981; *Wannamaker et al.*, 1987b). However, the amount of inversion studies using FEM in forward modelling is rather limited and if FEM is used the mesh and coding of the elements have generally been kept fixed during the inversion (e.g., *Oristaglio and Worthington*, 1980). But fixing the mesh geometry and the element codes have several significant disadvantages in the inversion procedure. First, computing the theoretical responses at many frequencies needs necessarily changes in the mesh composition because of the changes in the skin depths. The use of only one mesh structure can give inaccurate results due to a too coarse mesh or can waste too much CPU time due to an unnecessarily dense mesh. Therefore, the element sizes, i.e., the mesh structure, must be changed at the different steps of the inversion. Secondly, with the fixed mesh and element codes inversion is difficult and limited and can be performed only by optimising the conductivities in different fixed blocks. This can lead with hundreds of conductivity values needed in the block-type inversion to a highly unstable and ill-conditioned inverse problem. Thirdly, the proper fitting of the field data with the computed responses done during the inversion needs necessarily the possibility to move the subsurface targets in the mesh. This also means that the fixed mesh geometry is a severe limitation in a well working inversion procedure, as for example, the precise location of the target is then not possible.

In modelling of inhomogeneities in a stable and well-conditioned way during the optimisation of the model parameters we need an automatic mesh generation and element coding. Even though mathematically the automatic mesh generation has been during recent years a very popular research topic (e.g., *Ho-Le*, 1988; *George*, 1991; *Shimada and Gossard*, 1998), in some parts of computational physics, e.g. in electromagnetic inversion there is still a lack of proper approaches of an automatic FEM mesh generation and element coding. *Travis and Chave* (1989) have demonstrated the moving finite element method in 2-D MT modelling. However, this approach also does not serve directly the purpose needed in inversion. *Schnegg* (1993) described an automatic scheme for 2-D MT modelling based on lower order polynomial fitting. The approach discussed by *Schnegg* (1993) is quite interesting and is able to determine the varying thicknesses and resistivities in the columns (blocks) formed by the layered structures.

In the present paper we modify and develop further the well-tested and well-documented 2-D MT finite element program by *Wannamaker et al.* (1987a, 1987b) in such a way that an automatic mesh and element codes generation is possible. The

approach is quite general and can be used in optimisation of specific geometrical bodies provided the model is not too complicated, i.e., there are no overlapping bodies in the lateral direction. The efficacy of the scheme is demonstrated in forward modelling and in inversion of VLF EM data.

2. Theoretical VLF and VLF-R anomalies

The VLF method in geophysical applications uses the powerful radio stations, which work in the frequency band 15-30 kHz as a source for the primary field. At sufficiently large distances from the transmitting antenna the primary field can be considered to be a plane wave field. For the conventional VLF method, in which the tilt angle and the ellipticity of the magnetic polarisation ellipse are measured, it is sufficient to utilise the E-polarisation, in which the electric field is parallel with the strike of the geological inhomogeneity in the 2-D case. This means that in the field an attempt is made to select a transmitter as closely as possible in line with the geological strike.

The tilt angle, θ , which is the inclination of the major axis of the polarisation ellipse, and the ellipticity, e , which is the ratio of the minor to the major axis of the ellipse, are calculated by the formulae (Smith and Ward, 1974)

$$\tan 2\theta = \pm \frac{2(H_z / H_y) \cos \Delta\phi}{1 - (H_z / H_y)^2} \quad (1)$$

and

$$e = \frac{H_z H_y \sin \Delta\phi}{H_1^2}, \quad (2)$$

where H_z and H_y are the amplitudes, the phase difference $\Delta\phi = \phi_z - \phi_y$, in which ϕ_z is the phase of H_z and ϕ_y is the phase of H_y and $H_1 = |H_z e^{i\Delta\phi} \sin \theta + H_y \cos \theta|$. The tangent of the tilt angle and the ellipticity are good approximations to the ratio of the real component of the vertical secondary magnetic field to the horizontal primary magnetic field and to the ratio of the quadrature component of the vertical secondary magnetic field to the horizontal primary field, respectively (Paterson and Ronka, 1971). These quantities are called the real ($= \tan \theta \times 100 \%$) and imaginary ($= e \times 100 \%$) anomalies, respectively and they are normally expressed in percentage. Real and imaginary anomalies are considered in this study.

A VLF-R measurement deals with the horizontal electric field component and orthogonal horizontal magnetic field and it is possible to use both the E- and H-polarisation. In the present study we used the E-polarisation, where the electric field is parallel with the geological strike (the x-direction). The apparent resistivity ρ_a [Ωm]

and phase angle φ [$^\circ$] computed from horizontal electric field E_x and magnetic field H_y are given by the formulae (e.g. *Kaikkonen*, 1980):

$$\rho_a = \frac{1}{\omega\mu} \left| \frac{E_x}{H_y} \right|^2 \quad (3)$$

and

$$\varphi = \arctan \left[\frac{\text{Im}(E_x / H_y)}{\text{Re}(E_x / H_y)} \right], \quad (4)$$

where ω is the angular frequency of the VLF primary field and μ is the magnetic permeability of the subsurface.

The field component E_x in equations (3) and (4) is obtained by applying the finite element technique with the Galerkin process directly to the Maxwell's equations and other field components in equations (1) - (4) can be computed from Maxwell's equations by numerical differentiation. To solve the forward problem the magnetotelluric finite element program of *Wannamaker et al.* (1987a, 1987b) has been used after a slight modification for VLF purposes. For the details of the finite element modelling and VLF computation, papers by *Kaikkonen* (1979, 1980) and *Wannamaker et al.* (1987b) are referred.

3. The scheme

In the original program by *Wannamaker et al.* (1987b) the mesh is constructed (discretized) for a given subsurface resistivity structure according to the certain parameter values (such as the number of nodes in the y- and z-directions, Δy and Δz values and the distribution of the code numbers for the different resistivities) described manually by the user in the rather large input file. The user has to decide the proper Δy and Δz values, i.e., the inner texture of the mesh and the external mesh size based on the calculation of the skin depths with the given frequency and resistivity values. This manual operation must be repeated every time when the frequency or subsurface resistivities are varying (enough). Of course, this kind of procedure will not work when a real inversion will be done.

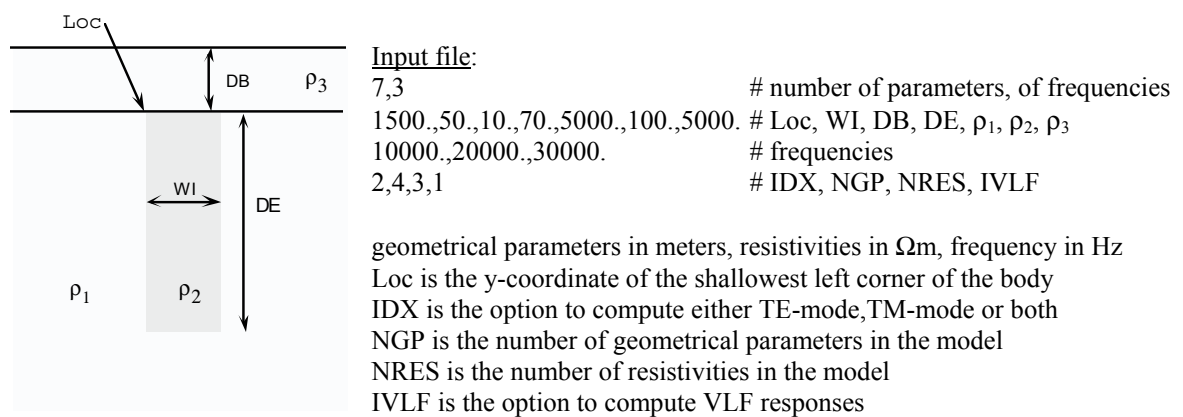
Our mesh construction for the EM problems is based on the physics, i.e., on the skin effect, of the problem and is free from any manual operation. When changes in the model parameters or in the frequency of the EM primary field appear the mesh is reconstructed automatically. The skin depth, δ , is the depth of penetration at which the electromagnetic field reduces to $1/e$ of its value at the surface of that medium (provided $\sigma \gg \omega\epsilon$) and is given by:

$$\delta = \left(\frac{2}{\omega \mu \sigma} \right)^{\frac{1}{2}} \text{ [unit of length]} \tag{5}$$

where ω , μ and σ are the angular frequency in rad, magnetic permeability in Hm^{-1} and electrical conductivity in Sm^{-1} , respectively.

Let us consider a simple dyke-like structure in a homogeneous half-space (Table 1). An input file needed to compute the forward solution for the model is also shown in Table 1. First we compute the skin depths δ_1 and δ_2 in the host and in the body, respectively. Then the body, starting from its left edge, is discretized in the y-direction into the elements whose width is $0.25\delta_2$. In this way the width of the rightmost element in the body may not have the same size as the other elements of the body. Now, when we know the amount of the elements (NEY) for the body we can equalise their width in the y-direction by dividing the width WI of the body by NEY. Next we have to determine the mesh structure in the host rock. On the both sides of the inhomogeneity within four elements, i.e., within about one δ_2 , the element width is kept the same as inside the body and after that it is increased gradually up to the distance of $5\delta_1$ multiplying the previous value by the factor of 1.5. In order to keep a control over the position of the body the width of the leftmost element should vary. Now the structure of the mesh and the number of the elements with the proper sizes and locations are determined in the y-direction. If the location, width or resistivity of the body or the resistivity of the host will change, the structure of the mesh must be changed accordingly. If the body is more resistive in comparison to the host then the discretization in and around the body is performed according to the host resistivity.

Table 1. Description of a simple model and the input file needed to compute the forward responses.



Next the discretization is determined in the z-direction. In order to keep an accuracy of the forward solution the mesh structure in the overburden, i.e., from the surface to the top of the shallowest body, is kept the same as in the body provided the body is the most conducting part in the model. If the overburden is the most conducting part in the structure then the discretization is performed according to the overburden

resistivity. If the thickness of overburden is so small that we cannot accommodate there at least 3 elements according to the skin depth rules then the discretization is reduced enough to be able to locate in the overburden that required minimum number (3) of elements against each resistivity. That demand is to fit galvanic or geometric components of the field (*Wannamaker et al., 1987a*). The element size in the vertical direction in the body is the same as in the lateral direction, i.e., $0.25\delta_2$. However, the element size can be a little smaller than $0.25\delta_2$ as the distance from the top to the bottom of the body is equalised to keep the element sizes the same in the body. Four elements, which means about one δ_2 , below the body are kept the same size. The host elements below one skin depth of the body are enlarged by a factor of 2.0 down to the bottom edge of the mesh at the depth of $5\delta_1$. Locating the external boundaries of the mesh at the distance of $5\delta_1$ from the nearest conductivity inhomogeneity was found to be a large enough distance. The original program code by *Wannamaker et al. (1987a, 1987b)* that defines the vertical mesh structure for the air above the Earth surface has not been changed. Now all the information to write the element codes according to the discretization of the subsurface resistivity structure is available and can be done automatically. Figure 1a shows the whole discretized mesh and Fig. 1b presents the part of the mesh around the body.

For a dipping body the discretization process follows mainly the procedure described above. As the FEM program by *Wannamaker et al. (1987a, 1987b)* uses as an input a triangle element varying dip angles also in the automatic generation is a rather straightforward step. We divide the whole rectangular area (Fig. 2a), which is defined by the dipping body, into the elements with the same lateral dimension, i.e., about $0.25\delta_2$, defined by the skin depth in the body. The vertical dimension of the element depends on the dip angle and δ_2 . If the vertical dimension calculated using the dip angle is getting larger than $0.25\delta_2$ then the lateral dimension is reduced properly to avoid too large vertical dimensions of the elements. This, of course, increases the CPU-time a little, but the accuracy in the solution is guaranteed better. Figure 2b shows the part of the mesh for the dipping body. It is important to mention that by equalising (see above) the top width of the body we can guarantee that the whole body (also every corner) is discretized laterally exactly by the elements with the same size. However, in the corner which has the smaller angle at the bottom edge of the body there can be the element which differs both laterally and vertically from the other elements of the body, i.e., the whole element row and column through that corner are different from the others discretized according to the dipping body.

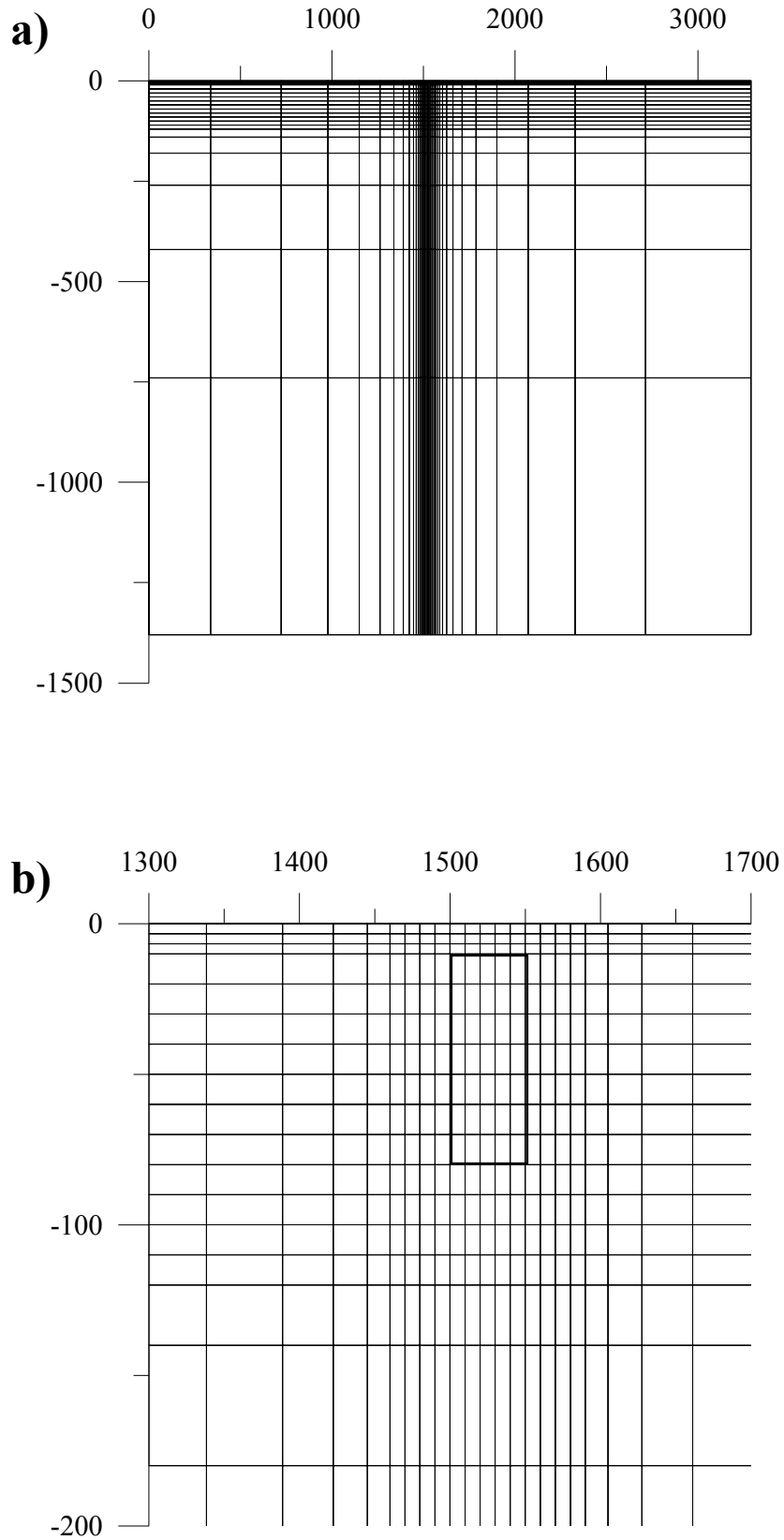


Fig. 1. **a)** Discretized mesh for the single vertical body and **b)** part of the mesh from around the body (thick line).

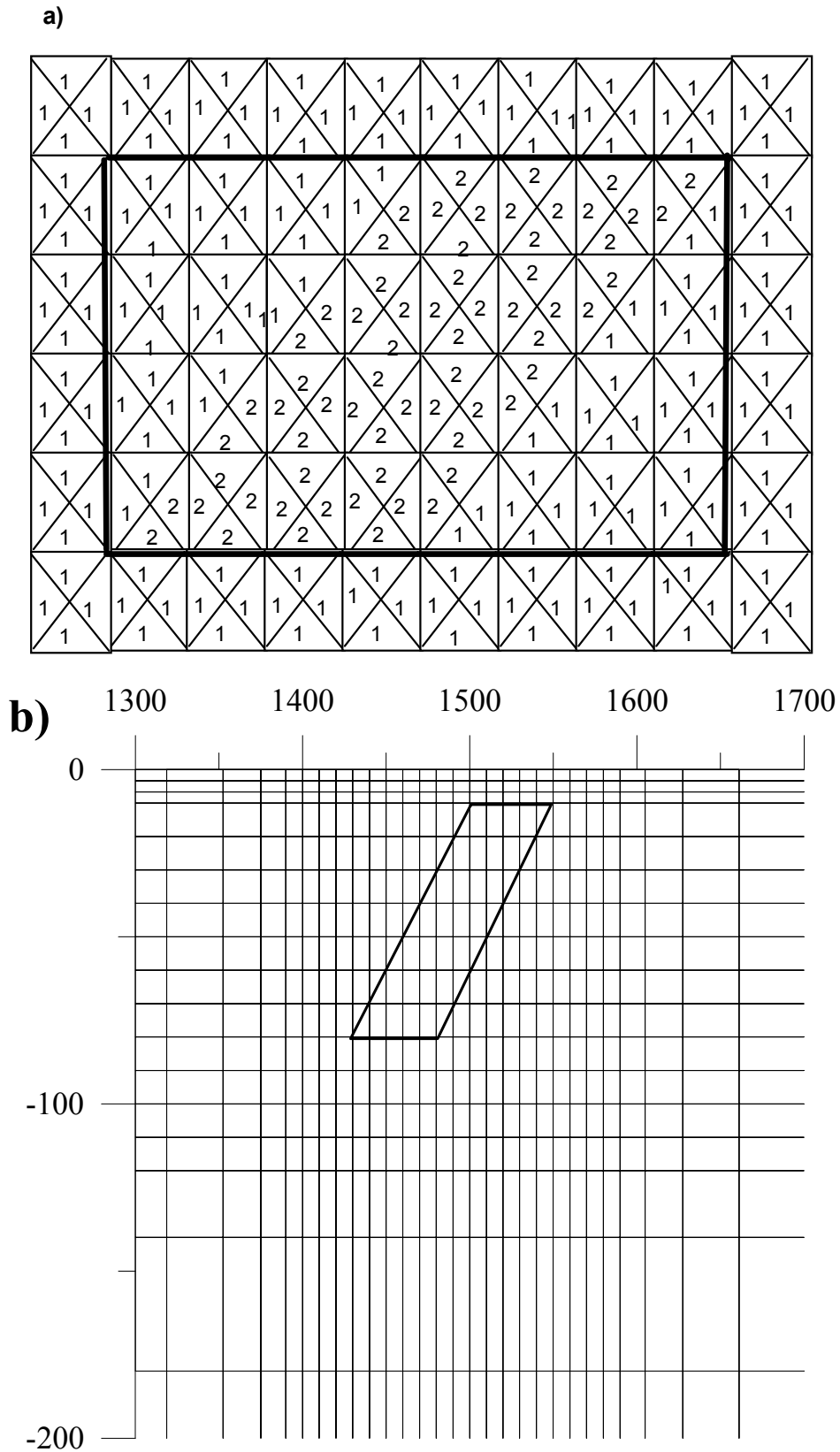


Fig. 2. **a)** The denser rectangular area defined by the triangles (with symbol 2) which form the dipping body and **b)** the part of the generated mesh around the body (thick line).

For the subsurface consisting of two or more inhomogeneities the automatic mesh generation can be done in the horizontal direction following the rules given above for a single body. However, in the vertical direction the discretization is done based on the skin depth of the most conducting target. This way is not the most economical one as it is possible that the rather large area is covered by the much too dense mesh, which correspondingly increases the CPU-time. However, this slight increase in the CPU-time is better than almost intractable difficulties in programming of the vertical discretization of really complex multi-body structures. Figures for the three-body model are presented later in the section 4.1.3.

The developed finite element mesh and code generation procedure is nothing else but the automatic reconstruction of the subsurface model, which is varying, in every new step of the optimisation process. Inversion would be impossible without this kind of automatization in the mesh and element code generation if we use FEM as the necessary forward modeller.

4. Results

4.1 Forward modelling examples

4.1.1 Single dyke

Figure 3a shows the model used in this example. Figures 3b, 3c and 3d show the parts of the meshes generated automatically for the model presented in Fig. 3a varying the resistivity of the body. The figures show how the scheme developed generates automatically the coarser meshes for the more resistive bodies (from Fig. 3b to Fig. 3d). The program keeps the meshes exactly the same for the resistivities of 50 Ωm and 100 Ωm in the lateral direction, but the mesh is changed in the vertical direction in the body. The reasons are first the demand to include at least three elements per inhomogeneity and second the rather thin body of 20 meters in width. The calculated VLF- and VLF-R responses are shown in Figs 3e (real anomaly), 3f (imaginary anomaly), 3g (apparent resistivity) and 3h (phase). True values of various model parameters shown in Fig 3a are given in Table 2 where the body resistivity (ρ_2) is varying 10, 50 and 100 Ωm respectively.

Table 2. Inversion results for the single-dyke model.

Parameters	True value	Search limits	Inversion results
Loc (m)	1500	1450-1550	1500.03
DB (m)	10	5-30	9.99
WI (m)	20	5-30	19.89
DE (m)	70	40-100	69.98
ρ_1 (Ωm)	5000	100-10000	4996.44
ρ_2 (Ωm)	10	1-100	9.94
ρ_3 (Ωm)	250	10-1000	249.73
Error	-	-	1.20E-07

4.1.2 Dipping dyke

Figure 4a shows the model used in the second example. In this example a 20 m thick body located at a depth of 10 m is dipping with an angle 45° in the host with resistivity 5000 Ωm . The body is extending 90 m (DE in Fig 4a) in vertical direction. Figures 4b, 4c and 4d show the parts of the meshes generated automatically for the dipping model in Fig. 4a varying the resistivity of the body. The figures show how the scheme again takes into account the varying resistivity of the body generating the denser meshes for the rectangular region formed by the more conducting body (Figs 4b, 4c and 4d). The computed responses are presented in Figs 4e, 4f, 4g and 4h.

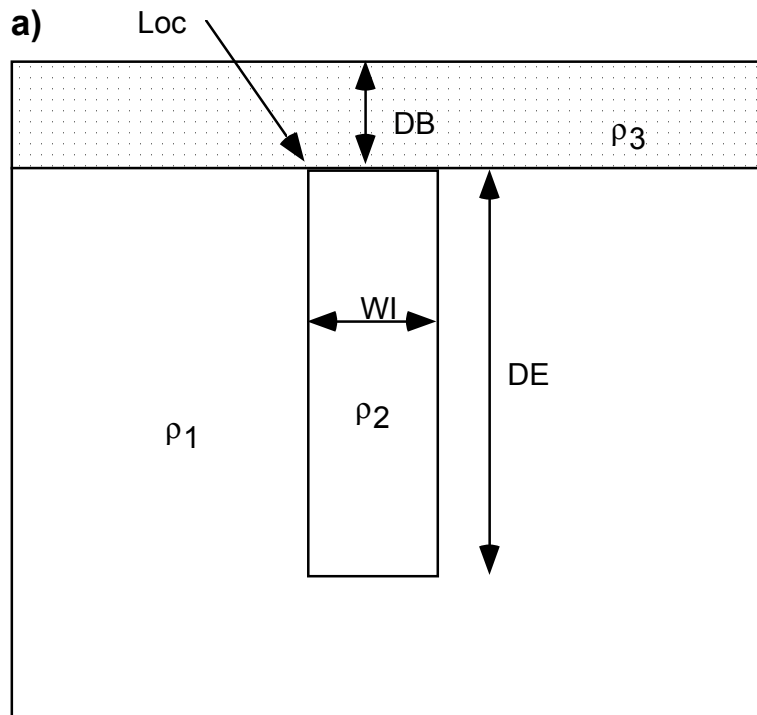


Fig. 3. **a)** Simple vertical dyke model. The part of the generated mesh for that model with **b)** 10 Ωm , **c)** 50 Ωm and **d)** 100 Ωm resistivity for the dyke. The computed **e)** real anomaly, **f)** imaginary anomaly, **g)** apparent resistivity and **h)** phase.

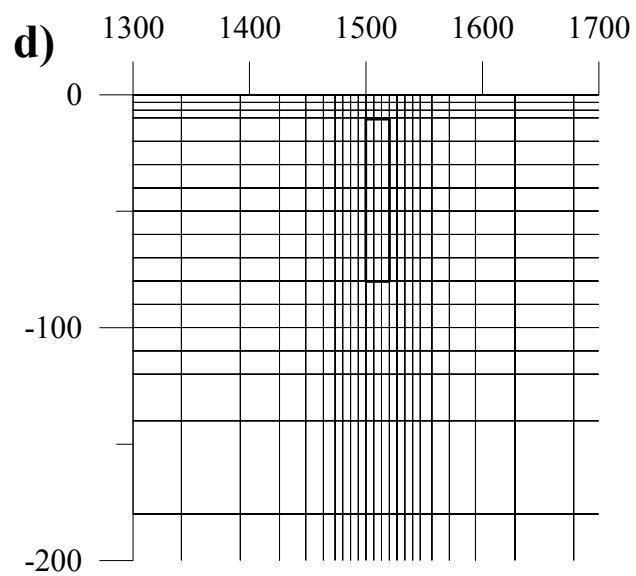
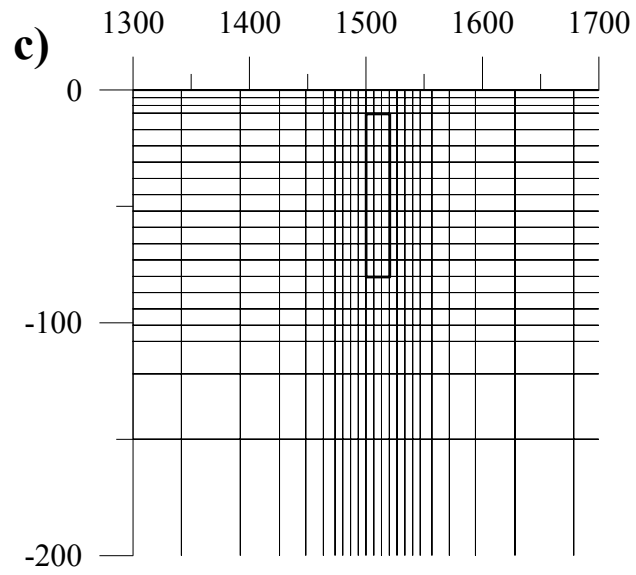
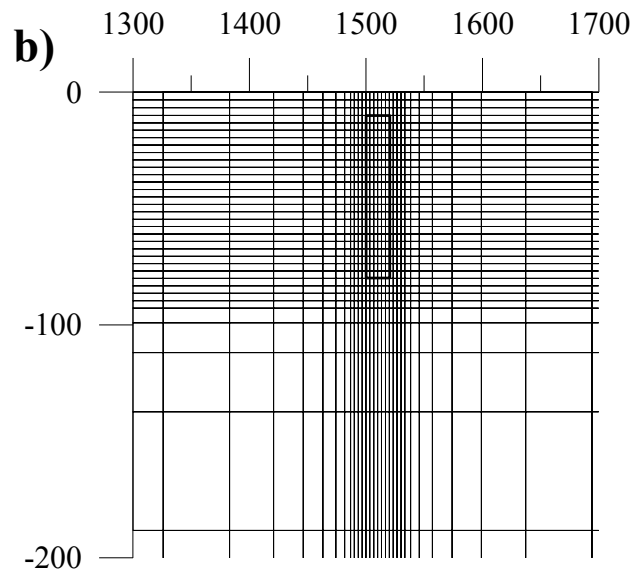


Fig. 3. Continued.

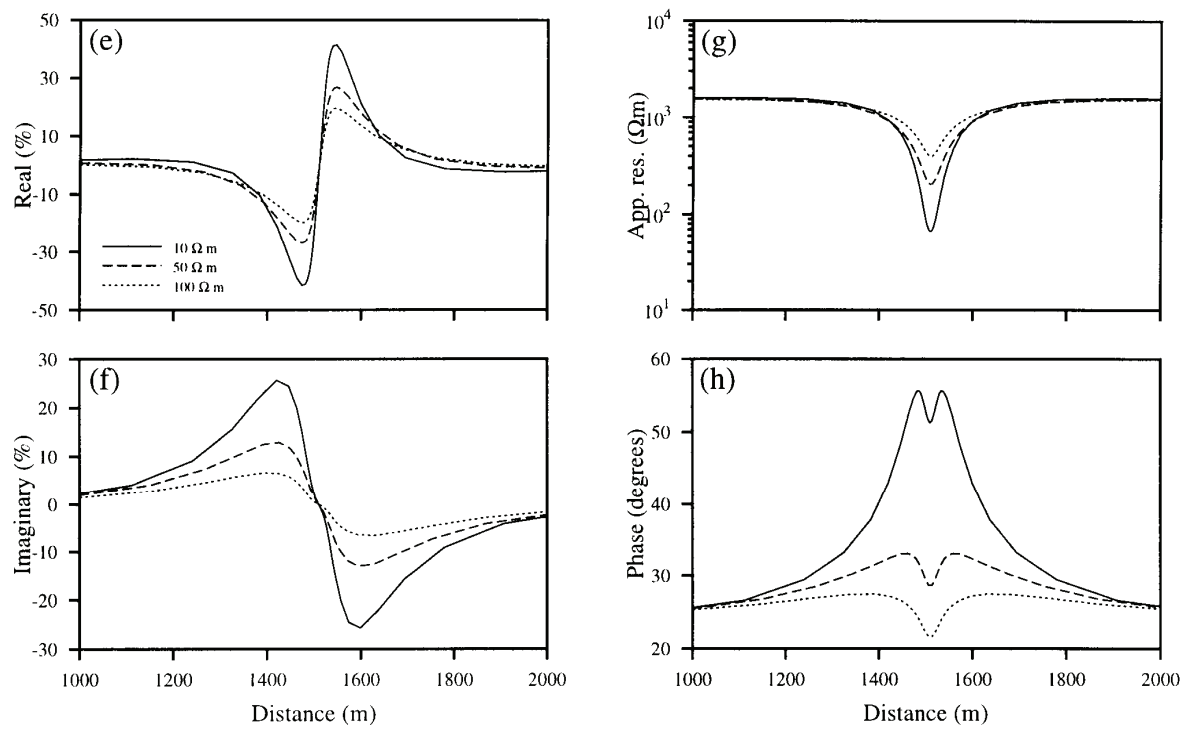


Fig. 3. Continued.

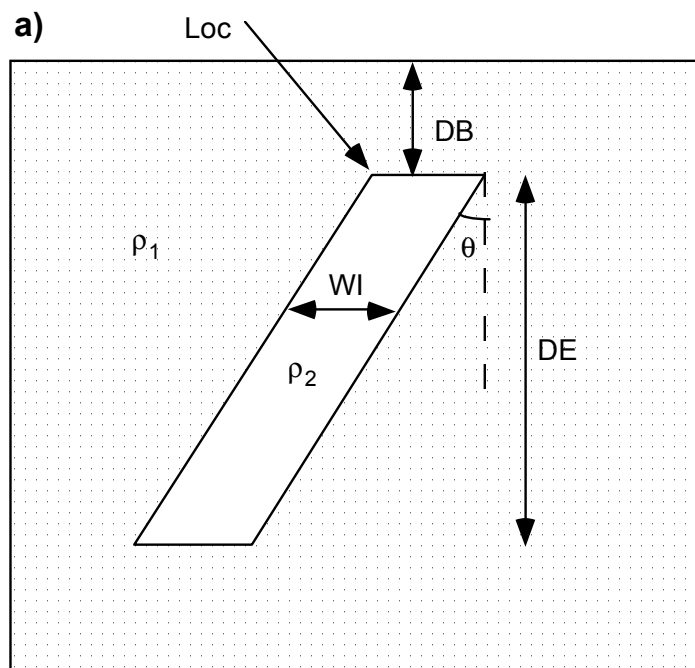


Fig. 4. **a)** Dipping dyke model. The part of the generated mesh for that model with **b)** 10 Ωm, **c)** 100 Ωm and **d)** 500 Ωm resistivity for the dyke. The computed **e)** real anomaly, **f)** imaginary anomaly, **g)** apparent resistivity and **h)** phase.

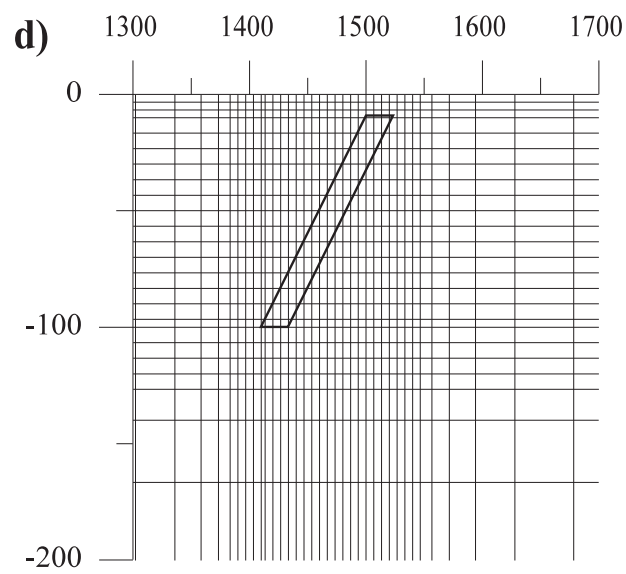
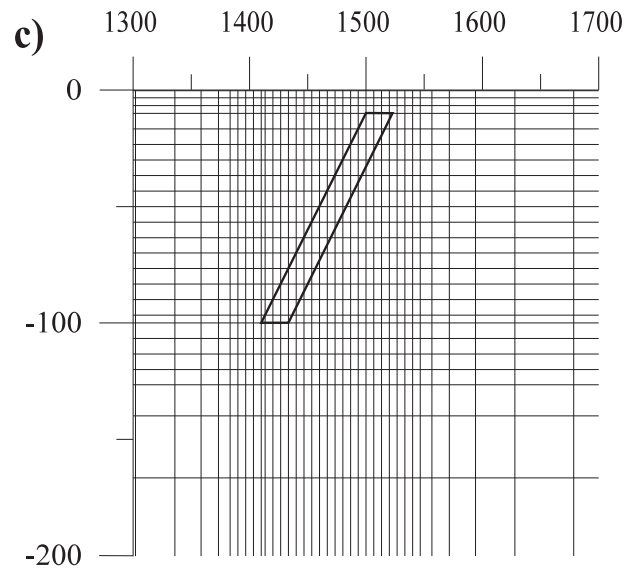
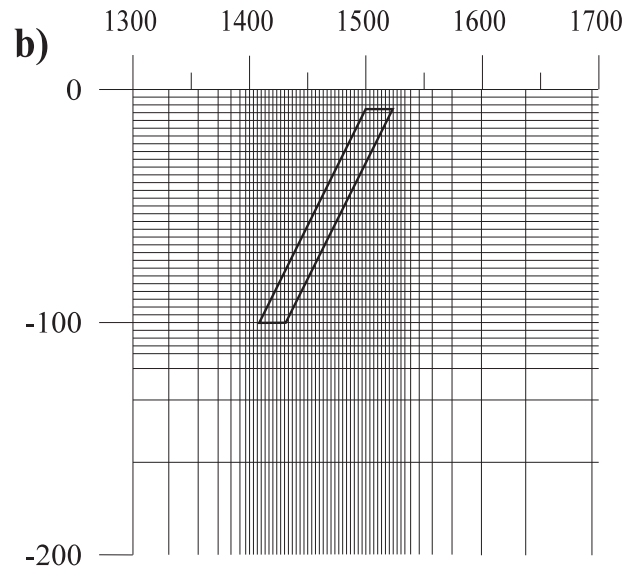


Fig. 4. Continued.

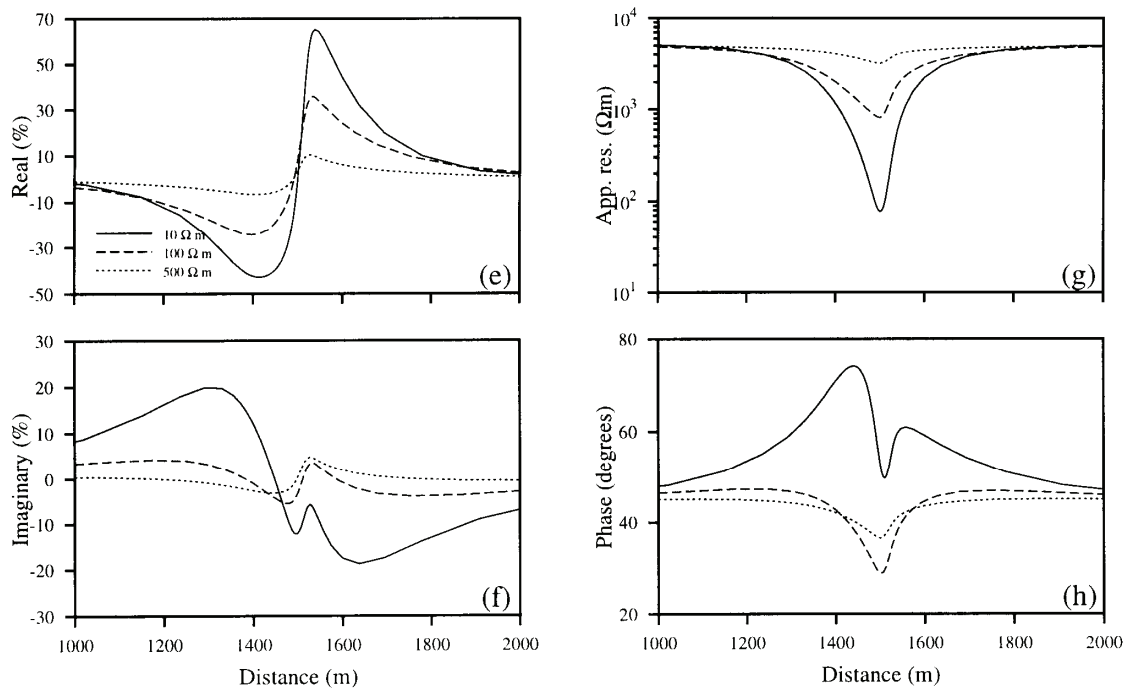


Fig. 4. Continued.

4.1.3 Three dykes

The more complicated model for testing our scheme is presented in Fig. 5a. True values of the model parameters shown in Fig 5a are given in Table 3 where the body resistivities ρ_3 and ρ_4 are interchanged for two different model computations. Figure 5b shows the part of the mesh generated for the model with the most conducting dyke (10 Ωm) at leftmost in Fig. 5a. Next we changed the resistivities of the dykes so that the most conducting body is located in the middle of the more resistive ones. Figure 5c shows how the scheme has worked automatically taking into account the changed resistivities by constructing the mesh to be denser now inside and around the most conducting dyke in the middle. The forward responses for these two cases are shown in Figs 5d, 5e, 5f and 5g.

Table 3. Inversion results for the three-dyke model.

Parameters	Truevalue	Search limits	Inversion results
Loc (m)	1500	1450-1550	1499.15
DB1 (m)	10	0-20	11.08
DB2 (m)	5	0-20	5.95
DB3 (m)	15	0-30	16.34
WI1 (m)	20	5-30	21.96
X1 (m)	300	100-400	302.19
WI2 (m)	10	5-30	15.52
X2 (m)	200	100-400	197.55
WI3 (m)	50	10-80	52.72
DE1(m)	50	25-100	50.05
DE2 (m)	60	25-100	59.36
DE3 (m)	70	25-100	73.18
ρ_1 (Ωm)	5000	100-10000	5028.92
ρ_2 (Ωm)	50	1-200	54.22
ρ_3 (Ωm)	500	10-1000	520.40
ρ_4 (Ωm)	10	1-200	14.78
ρ_5 (Ωm)	100	1-200	106.06
Error	-	-	6.32E-05

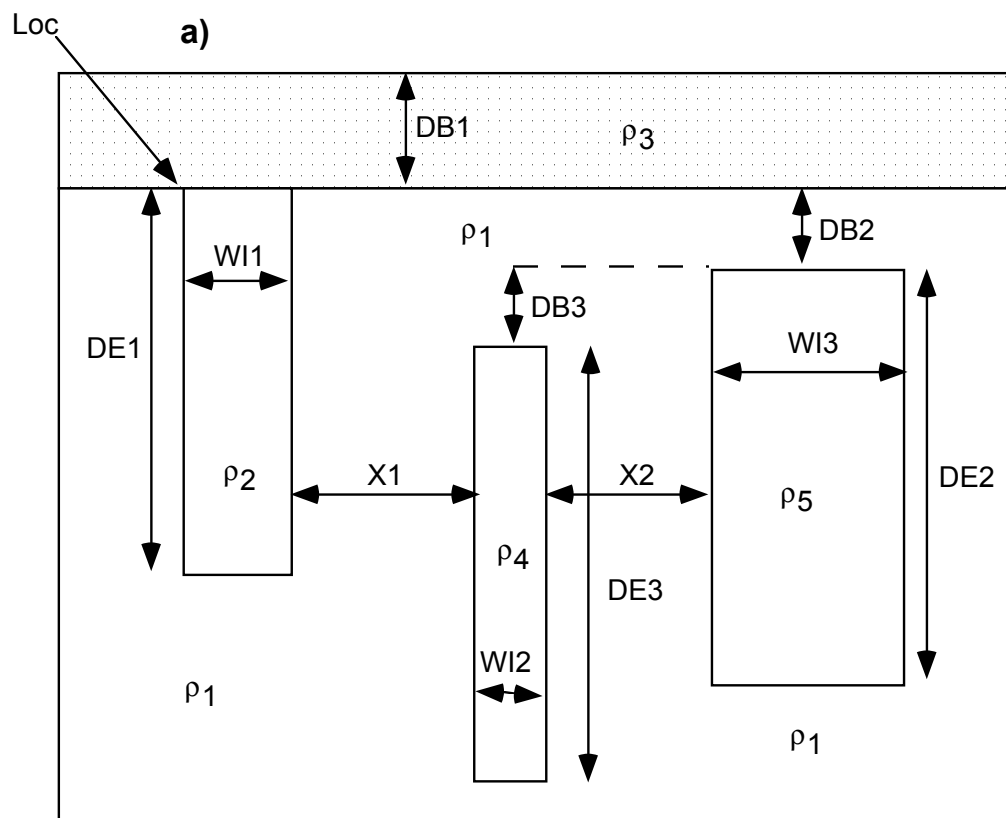


Fig. 5. **a)** Three-dyke model in forward modelling, **b)** the part of the mesh generated for the model with the most conducting dyke at leftmost, **c)** the part of the mesh for the most conducting dyke in the middle of the mesh and the computed **d)** real anomaly, **e)** imaginary anomaly, **f)** apparent resistivity and **g)** phase for these two models.

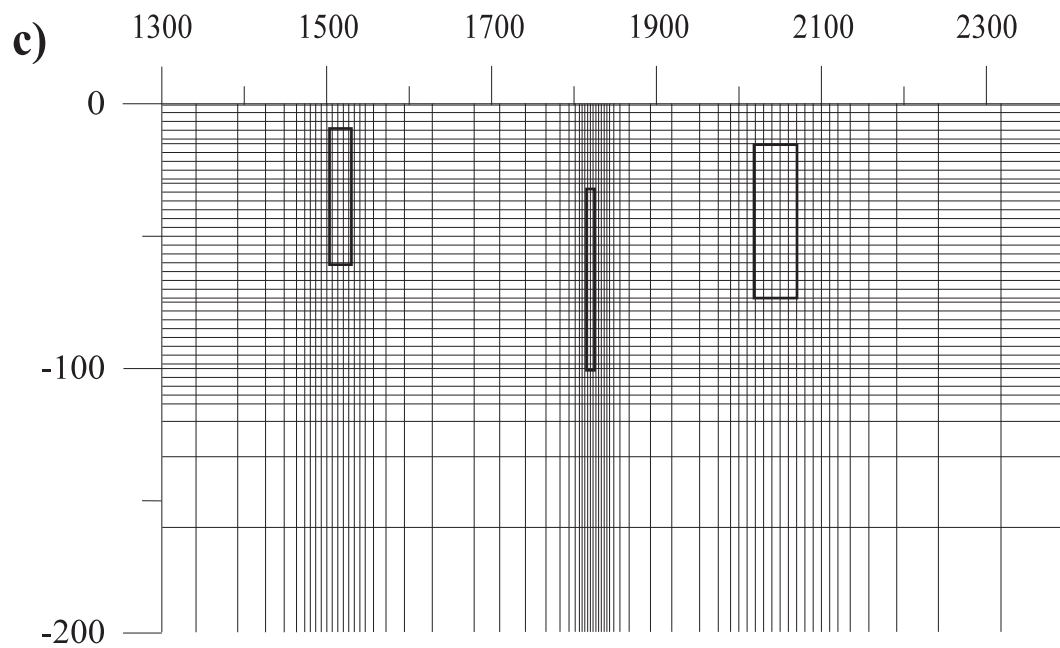
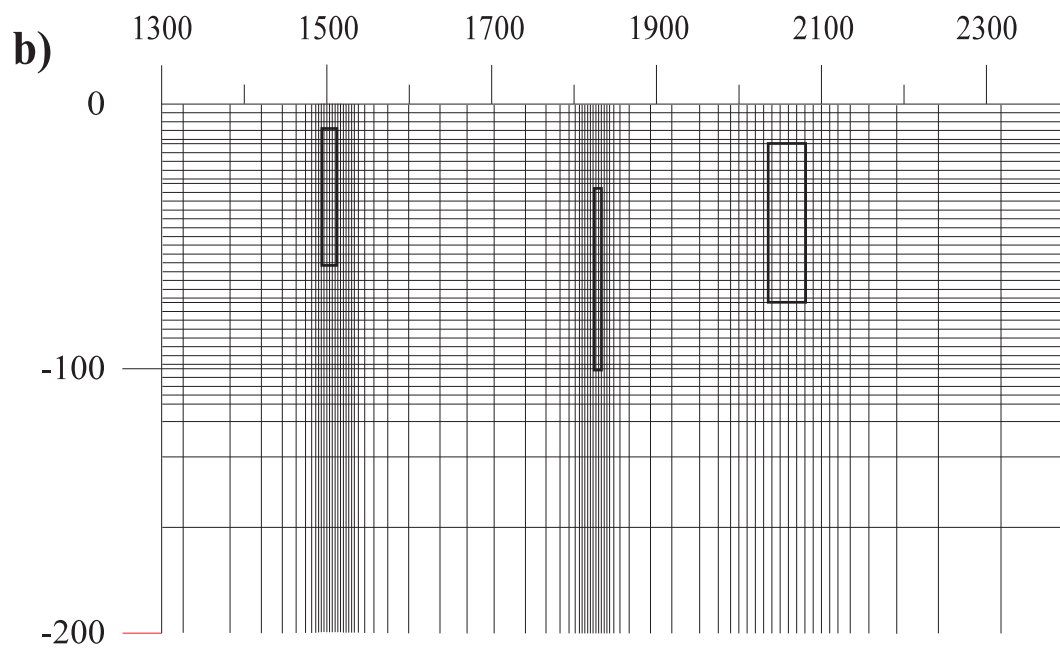


Fig. 5. Continued.

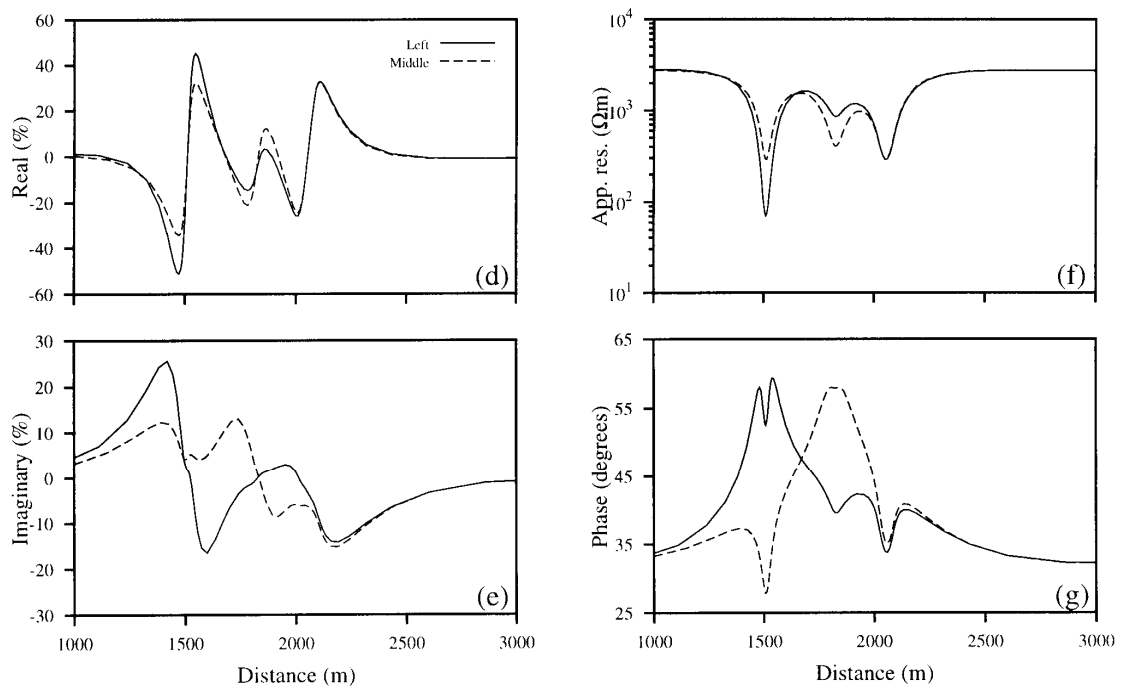


Fig. 5. Continued.

4.2 Inversion examples

To study the efficacy of the developed approach of automatic mesh generation and element coding in inversion process, we present here two examples, one for a simple and another for complex model. All the VLF and VLF-R data sets are jointly inverted using very fast simulated annealing (VFSA) global inversion technique. During the VFSA global inversion a new mesh is generated automatically for every 50000 models, i.e., due to 5 VFSA runs each of them consisting of 10000 models. Finally, the model parameters obtained after 5 VFSA runs are used to compute the mean model (see for details *Sen and Stoffa, 1995; Sharma and Kaikkonen, 1998*).

4.2.1 Single-dyke model

For this case we use the synthetic data generated by the model shown in Fig. 3a. We consider the VLF and VLF-R synthetic responses shown in Figs 3e, 3f, 3g and 3h corresponding to the resistivity of the body as $10 \Omega\text{m}$. The comparison of the synthetic VLF and VLF-R responses with the computed responses for the mean model obtained after 5 VFSA runs are shown in Figs 6a, 6b, 6c and 6d. These figures reveal an excellent agreement between the observed and computed responses. Table 2 shows the numerical values of the mean model parameters, their search limits and true values. Table 2 reveals that all the model parameters are resolved very well.

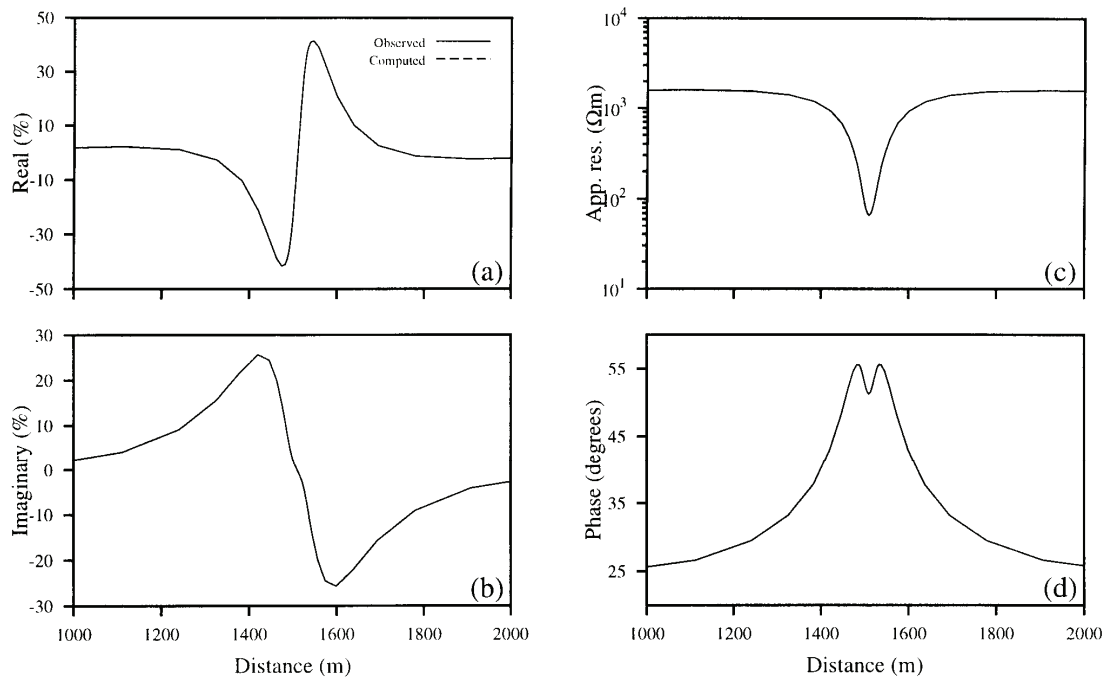


Fig. 6. Comparison of the observed responses with the computed responses for the mean model **a**) real anomaly, **b**) imaginary anomaly, **c**) apparent resistivity and **d**) phase, after the joint inversion of VLF and VLF-R data sets from a single-dyke model. Note the excellent agreement between the observed and computed responses.

4.2.2 Three-dyke model

In this case we deal with the synthetic data generated by the model shown in Fig. 5a with the change that the most conducting dyke is located in the middle. Figures 7a, 7b, 7c and 7d show the comparison between the observed and computed responses for the mean model after the joint inversion of all the VLF and VLF-R data. The figures reveal a good agreement between the observed and computed responses. Figures 8a, 8b and 8c show the conductivity cross sections for the true model, randomly selected initial model and the mean (final) model respectively. The conductivity cross-section corresponding to the mean model also shows a good agreement with that due to the true model. Table 3 presents the numerical values of the mean model obtained after inversion, their true values and search limits used during inversion.

In spite of the fact that the observed and computed responses are fitted extremely well, Table 3 reveals that the resistivity and the thickness associated with the most conducting dyke are not resolved properly. This is the problem associated with the nonuniqueness in geophysical interpretation. The solution of such ambiguities is not the aim of the present paper. For the inversion details we refer to the papers by *Sharma and Kaikkonen* (1998) and *Kaikkonen and Sharma* (1998). They deal with global inversion with VFSA and FEM in forward modelling for different types of synthetic, noisy and

field VLF and VLF-R data. The ambiguities associated with VLF and VLF-R data and their reduction are also discussed in those papers.

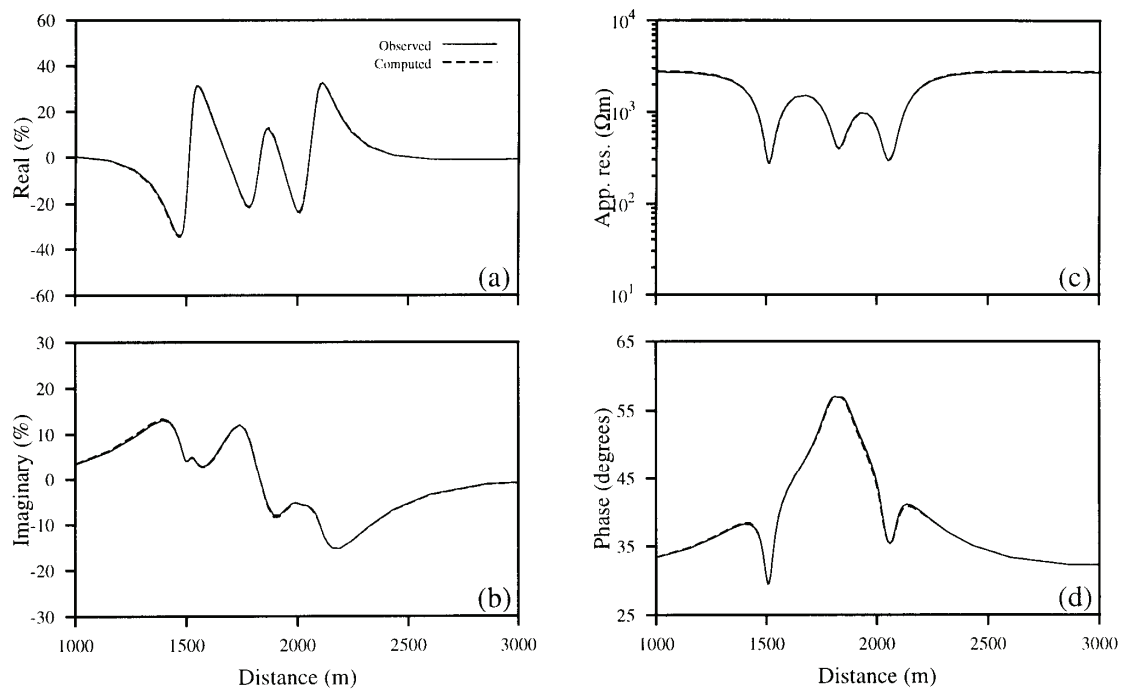


Fig. 7. Comparison of the observed responses with the computed responses for the mean model **a**) real anomaly, **b**) imaginary anomaly, **c**) apparent resistivity and **d**) phase, after the joint inversion of VLF and VLF-R data sets from three-dyke model.

4.3 CPU-time

The CPU-time needed in the single-dyke inversion example (with the approximate mesh size of 40×30 nodes) presented above was 24549 seconds. This CPU-time includes the mesh generation, element coding, forward solutions and other computations of inversion for all the 50000 models. The CPU-time needed in the second inversion example (the three-dyke model with the approximate mesh size of 120×90 nodes) to evaluate the same number of models was 89767 seconds. The CPU-times reported above are on the SUN Ultra Enterprise 4000 workstation for a single VLF frequency including, however, all VLF and VLF-R responses. Obviously, the CPU-time will be larger when more frequencies will be considered.

5. Conclusions

The 2-D MT finite element program by *Wannamaker et al.* (1987a, 1987b) has been developed further and modified in such a way that an automatic mesh and element code generation is possible. Our automatic mesh construction for the EM problems is based on the physics, i.e., on the skin effect, of the problem and is free from any manual

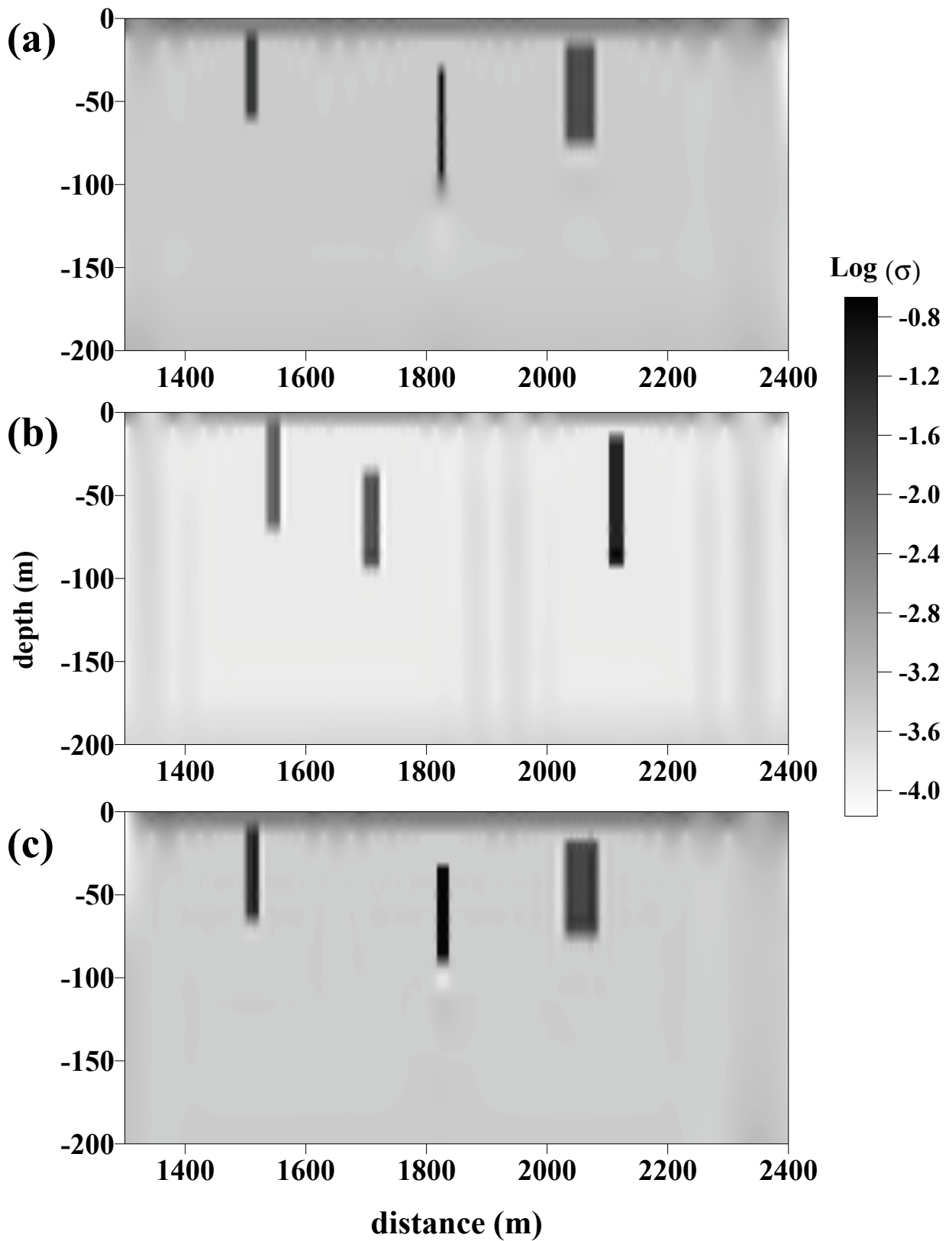


Fig. 8. Conductivity cross-sections for a) synthetic model, b) randomly selected initial model and c) mean model obtained after 5 VFSA runs.

operation. When changes in the model parameters or in the frequency of the EM primary field appear, the mesh is reconstructed automatically. The approach is quite general. However, the present version of the program cannot handle the structure, which consists of the bodies, which are overlapping, in the lateral direction. The discretization of the structure with the bodies overlapping in the vertical direction is carried out for the whole structure according to the most conducting body and therefore, even though working well, cannot be the most economical way for the computing resources. The automatic mesh and element code reconstruction is particularly useful, important and absolutely necessary in inversion with the FEM forward modelling.

Acknowledgements

The visit of SPS to Finland was made possible through support from CIMO (Centre for International Mobility) in Helsinki, Finland. The computations of this study were done using the computers Sun Enterprise Ultra 4000 of the Computing Centre of the University of Oulu. We thank two anonymous reviewers for their helpful suggestions and comments.

References

- Coggon, J.H., 1971. Electromagnetic and electrical modeling by the finite element method, *Geophysics*, **36**, 132-155.
- George, P. L., 1991. Automatic Mesh Generation: Application to Finite Element Methods, Wiley, New York, 333 pp.
- Ho-Le K., 1988. Finite Element Mesh Generation Methods: A Review and Classification, *Computer Aided Design*, **1**, No. 20, 27-38.
- Jupp, D.L.B. and K. Vozoff, 1977. Two-dimensional magnetotelluric inversion, *Geophys. J. R. Astr. Soc.*, **50**, 333-352.
- Kaikkonen, P., 1977. A finite element program package for electromagnetic modeling. *J. Geophys.*, **43**, 179-192.
- Kaikkonen, P., 1979. Numerical VLF modeling, *Geophysical Prospecting*, **27**, 815-834.
- Kaikkonen, P., 1980. Interpretation nomograms for VLF measurements. *Acta Univ. Oul. A 92. Phys.* 17, 48 pp.
- Kaikkonen, P. and S.P. Sharma, 1998. 2-D nonlinear joint inversion of VLF and VLF-R data using simulated annealing, *Journal of Applied Geophysics*, **39**, 155-176.
- Oristaglio, M.L. and M.H. Worthington, 1980. Inversion of surface and borehole electromagnetic data for two dimensional electrical conductivity models, *Geophysical Prospecting*, **28**, 633-657.
- Paterson, N.R. and V. Ronka, 1971. Five years of surveying with Very Low Frequency - Electro Magnetics method, *Geoexploration*, **9**, 7-26.

- Pridmore, D.F., G.W. Hohmann, S.H. Ward and W.R. Sill, 1981. An investigation of finite element modeling for electrical and electromagnetic data in three dimensions, *Geophysics*, **46**, 1009-1024.
- Reddy, I.K. and D. Rankin, 1973. Magnetotelluric response of a two-dimensional sloping contact by the finite element method, *Pure and Appl. Geophys.*, **105**, 847-857.
- Rodi, W.L., 1976. A technique for improving the accuracy of finite element solutions for magnetotelluric data, *Geophys. J. R. Astr. Soc.*, **44**, 483-506.
- Schnegg, P.-A., 1993. An automatic scheme for 2-D magnetotelluric modelling, based on low-order polynomial fitting, *J. Geomag. Geoelectr.*, **45**, 1039-1043.
- Sen, M. and P.L. Stoffa, 1995, Global optimization methods in geophysical inversion, Elsevier, Amsterdam, 281 pp.
- Sharma, S.P. and P. Kaikkonen, 1998. Two-dimensional non-linear inversion of VLF-R data using simulated annealing, *Geophysical Journal International*, **133**, 649-668.
- Shimada, K. and D.C. Gossard, 1998. Automatic triangular mesh generation of trimmed parametric surfaces for finite element analysis, *Computer Aided Geometric Design*, **15**, 199-222.
- Smith, B.D. and S.H. Ward, 1974. On the computation of polarization ellipse parameters. *Geophysics*, **39**, 867-869.
- Travis, B.J. and A.D. Chave, 1989. A moving finite element method for magnetotelluric modeling, *Phys. Earth Planet. Int.*, **53**, 432-443.
- Wannamaker, P.E., J.A. Stodt and L. Rijo, 1987a. PW2D - finite element program for solution of magnetotelluric responses of two-dimensional Earth resistivity structure. User Documentation. *Earth Science Laboratory, University of Utah, Research Institute, Salt Lake City, Revised Edition, ESL-158*, pp. 29+11
- Wannamaker, P.E., J.A. Stodt and L. Rijo, 1987b. A stable finite element solution for two-dimensional magnetotelluric modeling, *Geophys. J. R. Astr. Soc.*, **88**, 277-296.
- Weidelt, P., 1975. Inversion of two-dimensional conductivity structures, *Phys. Earth Planet. Int.*, **10**, 282-291.
- Zhdanov, M.S. and Iv. M. Varentsov, 1983. Interpretation of local two-dimensional electromagnetic anomalies by formalized trial procedure, *Geophys. J. R. Astr. Soc.*, **75**, 623-638.